Journal of Structural Biology 187 (2014) 215–222

Contents lists available at ScienceDirect

Journal of Structural Biology

journal homepage: www.elsevier.com/locate/yjsbi

Crystal structures of *Ophiostoma piceae* sterol esterase: Structural insights into activation mechanism and product release

Javier Gutiérrez-Fernández [a,1], María Eugenia Vaquero [b,1], Alicia Prieto [b], Jorge Barriuso [b], María Jesús Martínez [b,*], Juan A. Hermoso [a,*]

[a] Departamento de Cristalografía y Biología Estructural, Instituto de Química-Física "Rocasolano", CSIC, Serrano 119, 28006 Madrid, Spain
[b] Departamento de Biología Medioambiental, Centro de Investigaciones Biológicas, CSIC, Ramiro de Maeztu 9, 28040 Madrid, Spain

ARTICLE INFO

Article history:
Received 15 January 2014
Received in revised form 27 June 2014
Accepted 29 July 2014
Available online 7 August 2014

Keywords:
Fungal lipase/esterase
Activation mechanism

ABSTRACT

Sterol esterases are able to efficiently hydrolyze both sterol esters and triglycerides and to carry out synthesis reactions in the presence of organic solvents. Their high versatility makes them excellent candidates for biotechnological purposes. Sterol esterase from fungus *Ophiostoma piceae* (OPE) belongs to the family abH03.01 of the *Candida rugosa* lipase-like proteins. Crystal structures of OPE were solved in this study for the closed and open conformations. Enzyme activation involves a large displacement of the conserved lid, structural rearrangements of loop α16–α17, and formation of a dimer with a large opening. Three PEG molecules are placed in the active site, mimicking chains of the triglyceride substrate, demonstrating the position of the oxyanion hole and the three pockets that accommodate the *sn*-1, *sn*-2 and *sn*-3 fatty acids chains. One of them is an internal tunnel, connecting the active center with the outer surface of the enzyme 30 Å far from the catalytic Ser220. Based on our structural and biochemical results we propose a mechanism by which a great variety of different substrates can be hydrolyzed in OPE paving the way for the construction of new variants to improve the catalytic properties of these enzymes and their biotechnological applications.

1. Introduction

Triacylglycerol lipases (EC 3.1.1.3) are enzymes ubiquitous in nature, from microbes to plants and animals, catalyzing the hydrolysis of triglycerides to diglycerides, monoglycerides, free fatty acids and glycerol. In addition, these enzymes can catalyze esterification and transesterification reactions in the presence of organic solvents (Houde et al., 2004). Their interest is related to their application in a wide range of industrial processes: food, detergents, cosmetics, pharmaceutical, textile and paper industry (Reetz, 2002; Singh and Mukhopadhyay, 2012).

On the other hand, sterol esterases (EC 3.1.1.13) are defined as enzymes that hydrolyze sterol esters releasing free sterols and fatty acids. These enzymes were described in mammal tissues and in some fungi and bacteria (Rahim and Sih, 1969; Ghosh et al., 1995). Initially they were proposed to be used to detect cholesterol in blood (Allain et al., 1974) but their importance increased during the last decade since, in addition to their ability to hydrolyze sterol esters, they are able to hydrolyze triglycerides efficiently (Calero-Rueda et al., 2002b; Kontkanen et al., 2006; Maeda et al., 2008) and carry out synthesis reactions in the presence of organic solvents (Morinaga et al., 2011; Barba et al., 2011). Due to their high versatility, these enzymes proved to have high biotechnological interest for pitch reduction during paper pulp manufacture (Calero-Rueda et al., 2002a) and they can also catalyze the synthesis of phytosterol esters used as food additives (Morinaga et al., 2011; Barba et al., 2011).

Both lipases and sterol esterases are α/β-hydrolases showing a substrate-binding site formed by an extensive hydrophobic pocket (Grochulski et al., 1993; Mancheño et al., 2003). A traditional criterion accepted to define an enzyme as a lipase deals with the huge increase of their activity in the lipid–water interface, owing to a phenomenon known as interfacial activation (Verger, 1997), a process that can be also triggered by micelles (Hermoso et al., 1997, 1996). This property is linked usually to the existence of a

Abbreviations: *p*NPB, *p*-nitrophenylbutyrate; *p*NPL, *p*-nitrophenyl laureate; *p*NPP, *p*-nitrophenylpalmitate; CHAPS, 3-[(3-cholamidopropyl)dimethylammonio]-1-propanesulfonate; OPE, *Ophiostoma piceae* esterase; PEG, polyethylene glycol.

* Corresponding authors. Fax: +34 91 536 04 32 (M.J. Martínez), +34 915642431 (J.A. Hermoso).
E-mail addresses: mjmartinez@cib.csic.es (M.J. Martínez), xjuan@iqfr.csic.es (J.A. Hermoso).

[1] Equally contributed to this work.

http://dx.doi.org/10.1016/j.jsb.2014.07.007
1047-8477/

structural lid in these enzymes, allowing the access of the lipidic substrate to the catalytic site (Holmquist, 2000). Nevertheless, the existence of a lid seems not to be the single determinant for interfacial activation (Mancheño et al., 2003). In the case of sterol esterases, no much information is available since most of them have not been characterized.

The yeast *Candida rugosa* secretes a variety of closely related enzymes, referred as lipases or sterol esterases. In light of biochemical and structural studies, the best-characterized enzymes from this yeast (Lip1, Lip2 and Lip3) exhibit a high sequence identity among them (77–88%), but they differ in their substrate specificity on triglycerides and cholesterol esters. These differences in the affinity towards these compounds are explained by small changes in the hydrophobicity of the substrate-binding site and the lid region (Mancheño et al., 2003).

Sterol esterase from *Ophiostoma piceae* (OPE) (UniProt Id Q2TFW1) belongs to the family abH03.01 of the *C. rugosa* lipase like proteins (The Lipase Engineering Database http://www.led.uni-stuttgart.de/) for which 326 members have been sequenced and the three-dimensional structures of lipases from *C. rugosa* (Grochulski et al., 1993), the lipase from *Geotrichum candidum* (Schrag and Cygler, 1993) and the esterase from *Aspergillus niger* (Bourne et al., 2004) are the only members up to now reported.

Recently, we described a computational model of three-dimensional structure for OPE based on *C. rugosa* Lip1 and Lip3 structures (Calero-Rueda et al., 2009; Barriuso et al., 2013). OPE is more efficient than *C. rugosa* Lip3 against sterol esters (Barba et al., 2011). Our model indicated that differences in the tunnel region of these enzymes could be related with their catalytic efficiency differences (Calero-Rueda et al., 2009).

Therefore, the development of structural studies is essential to understand the catalytic properties of these enzymes. The use of native *O. piceae* enzyme did not produce crystals suitable for X-ray diffraction (Calero-Rueda et al., 2002b). In this work we present the three-dimensional structure of this enzyme, in its open and closed conformations, by using the deglycosylated form of the recombinant protein expressed in *Pichia pastoris*, more soluble than the native one (Barba Cedillo et al., 2012). The activation mechanism and substrate stabilization is here described. This represents a hotspot in this field, opening the way for the rational design of new improved variants for industrial applications and allowing fine tuning enzyme activity.

2. Material and methods

2.1. OPE expression, purification and characterization

The enzyme was over-expressed in *P. pastoris* and purified in a single hydrophobic chromatography step (Octyl-Sepharose cartridge, GE Healthcare), as previously reported (Barba Cedillo et al., 2012), although in this case the protein was eluted after addition of 18 mM CHAPS in 25 mM Tris–HCl pH 7.0. The purified enzyme was dialyzed against 25 mM Tris–HCl, pH 7 to reduce the detergent concentration below 0.5 μM and stored at −20 °C until used.

Purified OPE was subjected to Size Exclusion Chromatography (SEC) using a Superose 12 GL 10/300 (GE Healthcare) with 20 mM Tris–HCl pH 7 plus 0.15 M NaCl at 0.3 mL min^{-1} to separate the multimolecular forms of the purified protein. Dextran blue (2000 kDa), Ferritin (460 kDa), Aldolase (170 kDa), BSA (73 kDa), Ovalbumin (48.2 kDa) and Chymotrypsinogen A (19.5 kDa), (calibration kits, Amersham Pharmacia), were used as standards to calibrate the column. Before deglycosylation with Endoglycosidase H (Roche), OPE was dialyzed against sodium citrate buffer pH 5.5 and then incubated at 37 °C for 24 h, following the manufacturer's instructions. Deglycosylation was checked by SDS–PAGE, staining the protein bands with Coomassie R-250 or with silver reagent. The deglycosylated enzyme was dialyzed against 25 mM Tris–HCl, pH 7.0 for crystallization assays.

Enzyme activity against esters of *p*-nitrophenol was measured by monitoring the hydrolysis of *p*NPB, *p*NPL and *p*NPP. A 20 mM stock solution of the substrates was prepared in HPLC grade acetone. The assay mixture contained 2 mM substrate in 20 mM Tris–HCl, pH 7.0 buffer and 1% (v/v) Genapol X-100. The reactions were monitored at 410 nm at room temperature in a Shimadzu UV-1800, in the case of *p*NPP and *p*NPL with magnetic stirring. One unit of activity (1 U) is defined as the amount of enzyme releasing 1 μmol of *p*-nitrophenol (ε_{410} = 15,200 $M^{-1}cm^{-1}$) per minute under the defined conditions.

Protein concentration was determined by BCA bioassay (Thermo) using bovine serum albumin as standard.

Analytical ultracentrifugation was used to check the aggregation behavior of recombinant proteins and the possible transition state between of both closed and open protein forms (monomer and dimer, respectively). Measurements were performed in a XL-I analytical ultracentrifuge (Beckman-Coulter Inc.) equipped with UV–VIS and interference detection optics. Samples, in 25 mM Tris–HCl, pH 7.0, were centrifuged at 48,000 rpm and 20 °C using an An50Ti eight hole rotor and double-sector Epon-charcoal centerpieces. Differential sedimentation coefficient distributions $c(s)$ were calculated by least-squares boundary modeling of the experimental data using the program SEDFIT (version 12.44) (Schuck, 2000). The experiments were carried out, by using both the purified protein after hydrophobic chromatography (0.5 mg/mL), consisting in a mixture of aggregates states (principally monomer and dimer), and the monomer isolated after SEC (0.2 mg/mL). These proteins were analyzed in presence or absence of 5 mM dodecane sulfonyl chloride (Sigma–Aldrich), as enzyme inhibitor, and 5 mM of cholesteryl oleate, as enzyme substrate (after 30 min of incubation at room temperature). The enzyme inhibitor was prepared in isooctane, remaining in the samples at 0.5%, and the substrate was dissolved in 0.02% Genapol X-100 and 150 mM NaCl (final concentration).

2.2. Construction of an OPE mutant

The mutant I544W was constructed by site-directed mutagenesis. The mutation was introduced by polymerase chain reaction (PCR), using the expression plasmid pPIC9OPE as template (Barba Cedillo et al., 2012). Both a direct and a reverse primer were designed complementary to opposite strands of the same DNA region. The following primers were used (with indication of the changed triplets in bold): OPE I544W (Fw: 5′-CAACAAC**TGG**GGCATCTTCC-3′ and Rv: 5′-GGAAGATGCC**CCA**GTTGTTG-3′). PCRs (50 μL final volume) were carried out in a Mastercycler Pro S (Eppendorf) using 100 ng of template DNA, each dNTP at 250 μM, 125 ng of direct and reverse primers, 5 units of expand long template enzyme mix (Roche), and the manufacturer's buffer number 3. Reaction conditions were as follows: (i) 95 °C for 1 min; (ii) 18 cycles at 95 °C for 50 s, 55 °C for 50 s, and 68 °C for 10 min; and (iii) a final cycle at 68 °C for 10 min. After amplification, the PCR products were treated with DpnI restriction enzyme (Roche) to digest the parental strand. The mutated gene was completely sequenced using an ABI 3730 DNA analyzer (Applied Biosystems) to ensure that only the desired mutation was introduced.

2.3. Crystallization and data collection

Initial crystallization trials were performed by the sitting drop vapor-diffusion method at 18 °C. A wide range of crystallization conditions were assayed by high-throughput techniques, using a NanoDrop robot with Innovadyne SD-2 microplates (Innovadyne

Technologies Inc., California, USA). The mixture contained 250 nL of protein solution and 250 nL of precipitant solution, equilibrated against 65 μL of well solution. Successful crystallization conditions were optimized by a hanging-drop vapor-diffusion method, mixing 1 μL of protein solution and 1 μL of precipitant solution, equilibrating against 500 μL of reservoir solution. Native OPE was assayed at 10 mg mL^{-1} in 25 mM Tris–HCl pH 7.0 (Sigma–Aldrich). Two different habits were found in different conditions. Optimized habit I crystals grew in 0.2 M sodium nitrate (Sigma–Aldrich), 0.1 M bis-tris propane pH 7.5 (Sigma–Aldrich) and 20% (w/v) PEG 3350 (Sigma–Aldrich), while habit II crystals grew in 10% (v/v) 1,4-dioxane (Sigma–Aldrich), 0.1 M MES pH 6.5 (Sigma–Aldrich) and 1.6 M ammonium sulfate (Sigma–Aldrich). Native datasets of both habits were collected, using synchrotron radiation, at beamline ID29 in the ESRF (Grenoble, France) and cryoprotected with 20% glycerol (Sigma–Aldrich). Both datasets were processed with XDS (Kabsch, 2010) and scaled with SCALA (Evans, 2006), from CCP4 suite (Winn et al., 2011). Habit I crystals diffracted up to 2.0 Å resolution and belonged to the tetragonal $I4_1$ space group ($a = b = 164.12$ Å, $c = 93.99$ Å; $\alpha = \beta = \gamma = 90°$). A dimer was found in the asymmetric unit, with a Matthews' coefficient of 2.67 $Å^3\ Da^{-1}$ and a solvent content of 54.03%. Habit II crystals diffracted up to 2.6 Å resolution and belonged to the hexagonal $P6_322$ space group ($a = b = 119.27$ Å, $c = 206.77$ Å; $\alpha = \beta = 90°$, $\gamma = 120°$). One single monomer was found in the asymmetric unit, with a Matthews' coefficient of 3.44 $Å^3\ Da^{-1}$ and a solvent content of 64.24%.

2.4. Structure determination and refinement

Structure associated to habit I was solved by molecular replacement with Phaser (McCoy et al., 2007), using *C. rugosa* Lip1, PDB code 1LPN, sequence identity = 42.8%; (Grochulski et al., 1994), as initial model. The resulting structure was used as initial model to solve, by molecular replacement, the structure associated to the habit II. The refinement and manual model building of both structures was carried out with Phenix (Adams et al., 2010) and Coot (Emsley et al., 2010), respectively. Figures involving structural elements of these proteins have been created in PyMOL (Schrödinger, 2010) and some surface representations have been designed with Hollow (Ho and Gruswitz, 2008).

The refinement converged to final values of $R_{work} = 0.17$ and $R_{free} = 0.21$ for habit I structure, and of $R_{work} = 0.17$ and $R_{free} = 0.22$ for habit II structure. The final model of habit I crystals presents 538 amino acids for one monomer and 537 amino acids for the other, showing both an open conformation. In addition, two N-Acetylglucosamine molecules have been modeled at the glycosilation sites of chain A. In chain B, only one site could be modeled with one additional NAG molecule. Two phospholipid molecules were clearly identified at the interphase between both chains in the active conformation. As they were not present in the crystallization conditions, we think that these molecules come from the purification stage. Since the real nature of these phospholipids was not determined, we have built a ligand in which the number of carbon atoms corresponds to the length of the electronic density at 0.8σ. Finally, some polyethilenglycol (PEG) molecules have been found and modeled. Surrounding chain A, we have modeled one molecule of pentaethilene glycol, three molecules of triethilene glycol and one molecule of di(hidroxiethil)ether. In chain B we have modeled four molecules of di(hidroxiethil)ether and one molecule of triethilene glycol. Habit II crystals contained the closed conformation of the enzyme which presents 538 amino acids. Contrary to open conformation, no ligands were found in habit II structure. Structural determination parameters and refinement statistics are summarized in Table 1.

Table 1
Data collection and refinement statistics[*].

	OPE[c]	OPE[o]	OPE-I544W
Data collection			
Space group	$P6_322$	$I4_1$	$I4_1$
Cell dimensions			
a, *b*, *c* (Å)	119.27, 119.27, 206.77	164.12, 164.12, 93.99	164.9, 164.9, 94.14
α, β, γ (°)	90, 90, 120	90, 90, 90	90, 90, 90
T (K)	100	100	100
Wavelength (Å)	0.97908	0.97908	1.00000
Resolution (Å)	46.2 (2.7–2.6)	43.6 (2.1–2.0)	58.3 (2.5–2.4)
No. unique reflections	26,901	84,190	49,299
R_{pim} (%)[a]	8.9 (49.2)	4.5 (32.8)	5.0 (43.3)
$\langle I/\sigma(I)\rangle$	6.9 (1.9)	11.7 (2.5)	12.5 (1.9)
Completeness (%)	98.5 (98.2)	100 (100)	99.7 (97.6)
Redundancy	3.4 (3.4)	7.0 (7.1)	6.8 (6.8)
Refinement			
Resolution (Å)	46.22–2.6	43.56–2.0	58.3–2.4
R_{work}/R_{free}[b]	0.17/0.22	0.17/0.21	0.20/0.25
R.m.s. deviations			
Bond length (Å)	0.007	0.008	0.010
Bond angles (°)	1.078	1.051	1.480
PDB code	4BE4	4BE9	4UPD

[*] Values in parentheses correspond to the highest resolution shell.

[a] $R_{pim} = \Sigma_{hkl}[1/(N-1)]^{1/2}\ \Sigma_i|I_i(hkl) - [I(hkl)]|/\Sigma_{hkl}\Sigma_i I_i(hkl)$, where $\Sigma_i I_i(hkl)$ is the *i*th measurement of reflection *hkl*, $[I(hkl)]$ is the weighted mean of all measurements and *N* is the redundancy for the *hkl* reflection.

[b] $R_{work}/R_{free} = \Sigma_{hkl}|F_o - F_c|/\Sigma_{hkl}|F_o|$, where F_c is the calculated and F_o is the observed structure factor amplitude of reflection *hkl* for the working/free (5%) set, respectively.

Crystallization of OPE I544W mutant was assayed at 9.5 mg mL^{-1} in 25 mM Tris–HCl pH 7.0 (Sigma–Aldrich) and crystals were obtained in 0.2 M sodium nitrate (Sigma–Aldrich), 0.1 M bis-tris propane pH 7.5 (Sigma–Aldrich) and 20% (w/v) PEG 3350 (Sigma–Aldrich), showing a shape similar to habit I. Diffraction datasets for the OPE I544W mutant were collected using synchrotron radiation, at beamline I03 in Diamond Light Source (Oxfordshire, UK). Datasets were processed with XDS (Kabsch, 2010) and scaled with SCALA (Evans, 2006), from CCP4 suite (Winn et al., 2011). OPE I544W mutant crystals diffracted up to 2.4 Å resolution and belonged to the tetragonal $I4_1$ space group ($a = b = 164.86$ Å, $c = 94.14$ Å; $\alpha = \beta = \gamma = 90°$). A dimer was found in the asymmetric unit, with a Matthews' coefficient of 2.68 $Å^3\ Da^{-1}$ and a solvent content of 54.08%.

The structure of OPE I544W mutant was solved by molecular replacement with Phaser (McCoy et al., 2007), using the previously solved open conformation from OPE as a model. The refinement and manual model building of OPE I544W mutant was carried out with Phenix (Adams et al., 2010) and Coot (Emsley et al., 2010), respectively. The refinement converged to final values of $R_{work} = 0.20$ and $R_{free} = 0.25$. The OPE I544W mutant shows the open conformation and also contains two phospholipids located in the interphase between both chains. Two NAG molecules have been modeled at the glycosilation sites of chain A and one more in chain B. Regarding the PEG chains observed in OPE, only one molecule of triethilen glycol has been modeled inside the tunnel of chain A. Chain B of OPE I544W showed higher B factors than in the open conformation of wild type OPE. Structural determination parameters and refinement statistics are summarized in Table 1.

2.5. Accession numbers

Coordinates and structure factors have been deposited in the Protein Data Bank with accession numbers 4BE9 and 4BE4 for the OPE open and closed conformations, respectively and 4UPD for the OPE-I544W mutant.

3. Results and discussion

3.1. Overall structure

Two different three-dimensional structures are presented in this report, namely, the structure of OPE in its closed conformation (OPE^c) (Fig. 1a) obtained from habit II crystals and the open conformation of the enzyme (OPE^o) (Fig. 1b) from habit I crystals. Crystal structure of OPE^c follows the protein scaffold of lipases from *C. rugosa* based on an αβ hydrolase fold (Ollis et al., 1992) with a major 11-stranded mixed β-sheet, a small and nearly perpendicular N-terminal 3-stranded β-sheet and 16 helices (Fig. 1a). The major β-sheet, which forms the core of the lipase, exhibits a pronounced twist, being the first (β_0) and last (β_{10}) strands almost perpendicular to each other. In agreement with this, lipase 2 of *C. rugosa* (PDB code 1GZ7, Mancheño et al., 2003) is the closest structural homologue of OPE^c (sequence identity = 42.5%, rmsd = 0.81 Å for 538 Cα atoms, Fig. S1 Supp. Mat.). OPE^c presents a 37 amino acids lid covering the active site. The lid consists of one α-helix (residues 83–88) and two 3_{10}-helices (residues 90–94 and 96–98) flanked by two loops that end in a disulfide hinge (from Cys72 to Cys108, Fig. 1c). OPE lid differs from that reported for *C. rugosa* and *G. candidum*. While the lid in *C. rugosa* Lip1 and Lip2 contains one α-helix of 10 residues and one 3_{10}-helix of 3 residues, the lid in *G. candidum* is formed by three α-helices containing 12, 4 and 10 residues, respectively.

A hydrophobic patch, formed by Ile407, Phe408, Phe458, Pro459 and Phe460, is located close to the lid (Fig. 1c). This Phe-Pro-Phe pattern appears only in OPE and not in the closest homologues. Both phenylalanines closely interact with some residues of the lid (Leu88 and Leu92).

The main structural difference between closed and open structures is the displacement of the lid up to about 30 Å away from its original position (Fig. 1c and Fig. S2 Supp. Mat.). This movement involves a rearrangement of its secondary structure that upon activation presents two α-helices (residues 84–93 and 96–101). A similar rearrangement is observed for the lipases/esterases from *C. rugosa*, but OPE presents the largest lid displacement among related enzymes (~30 Å in the longest separation) (Fig. S3 Supp. Mat.). Analysis of both OPE forms (habit I and II) indicates that the lid regions in the closed conformation is not involved in crystal contacts, while the lid in the open conformation is involved in oligomeric arrangement. In agreement with that, observed B-factors are higher for the lid in the closed conformation than in the open (Fig. S4 Supp. Mat.).

3.2. Oligomeric arrangement in OPE

A dimeric arrangement was observed for the open conformation OPE^o as also reported for crystal structures of the open forms of Lip1 (Grochulski et al., 1993) and Lip3 (Ghosh et al., 1995).

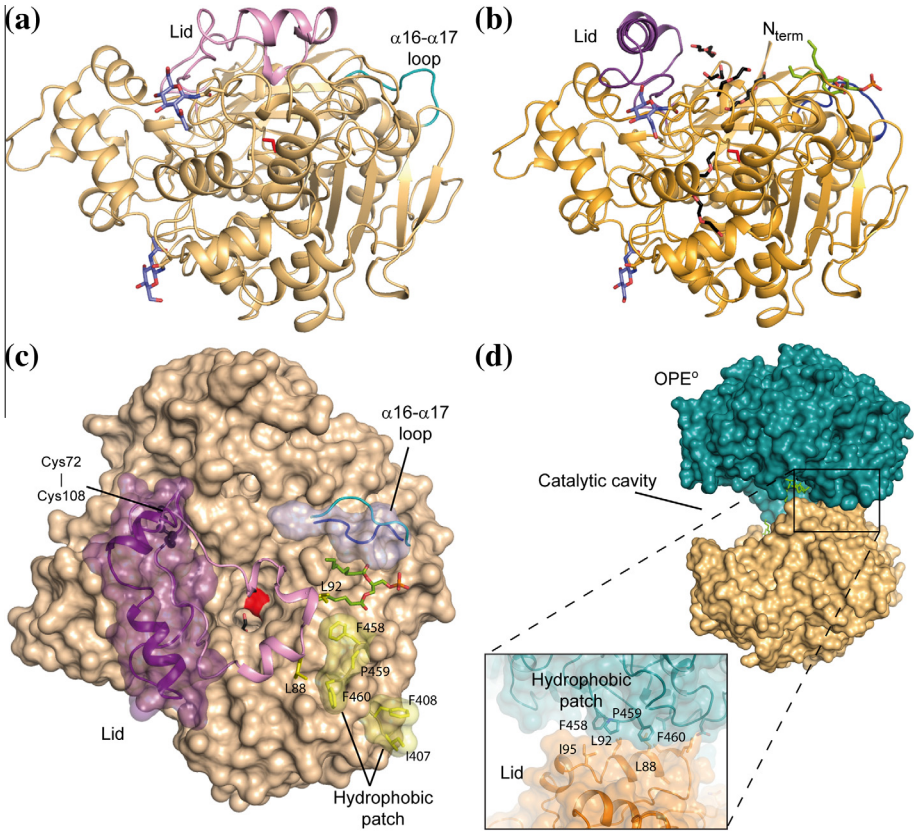

Fig.1. Overall structure of the closed and open conformations of OPE. (a) View of the closed OPE structure with the α/β hydrolase core colored in yellow and the lid colored in magenta. Glycan molecules attached to the glycosylation sites are represented as blue sticks. Catalytic Ser220 is shown in blue sticks. The α16–α17 loop is labeled. (b) View of the open OPE structure with the αβ hydrolase core colored in yellow and the lid colored in magenta. Glycan molecules attached to the glycosylation sites are represented as blue sticks. Catalytic Ser220 is shown in blue sticks. PEG chains are shown as black sticks and the phospholipid as green sticks. (c) Detailed view of the changes between closed and open states in OPE at the entry channel. Large displacements are observed for Val476 (9 Å) and for Leu477 (4 Å) between the closed (blue) and open (magenta) states. (d) Dimeric form of OPE in its open conformation, showing the catalytic cavity and the non-bonded contacts between the open lid of one chain and the hydrophobic patch of the other.

However, in contrast with that observed for Lip1 and Lip3 which monomers tightly associate forming dimers, OPE^{o} presents a dimer associated by regions in which aliphatic residues from the lid of one chain (Leu84, Leu85, Leu88, Leu92 and Ile95) interact with the hydrophobic patch of the opposite chain (Fig. 1d) with few contacts between OPE^{o} monomers and presenting a large cavity opened to the solvent (about 23 Å × 38 Å). Ultracentrifugation experiments carried out with native *O. piceae* enzyme showed protein multi-aggregates in aqueous solution while, in the same conditions, monomeric and dimeric forms were observed in the protein expressed in *P. pastoris* (Barba Cedillo et al., 2012).

Analytical ultracentrifugation studies (Table 2) showed a change in the percentages of monomer and dimer in the presence of inhibitor or substrate enzyme. In both cases, the purified OPE or monomeric-rich fraction, the predominant form was the monomer. In the presence of both, enzyme inhibitor or substrate, a significant amount of the monomer was converted into the dimer, suggesting the transition from the closed to the open enzyme form in the presence of both, inhibitor or substrate. The phenomenon of transition between the two conformations has been previously described in *C. rugosa* lipases, where exposure of the monomeric form of the enzyme to triolein dramatically accelerated its transition to the open form (Turner et al., 2001).

3.3. Activation mechanism in OPE

Besides opening of the lid, activation in OPE involves changes in the conformation of the loop α16–α17 (residues Tyr474–Tyr480), that stabilizes a phospholipid molecule located at the interface between both monomers of the dimer into a groove (11 Å wide, 8 Å deep and 15 Å long) connecting the outer part of the enzyme to the active site (Figs. 1c and 2). This phospholipid was not included in the crystallization conditions and very likely was incorporated during the purification process (see Section 2). A twist in Pro478 residue causes the displacement of the entire loop, with displacements of 9 Å in Val476 and 4 Å in Leu477 with regard to OPE^{c}, increasing the interactions with the lipid found in this groove (Fig. 1c). H-bond interactions affecting residues at the extremes of the loop (Asn479, Tyr480 and Tyr474 in Fig. S3 Supp. Mat.) serve as anchoring point for the α16–α17 loop. Structural analysis also provides indications about what could trigger lid movement. In OPE^{c}, Leu92 is lying on the entry channel and interacting with Phe458 and Phe464 from the hydrophobic patch. Upon activation, the position of Leu92 is now occupied by one of the aliphatic chains of the phospholipid (Fig. 2a).

Amino acid composition of loop α16–α17 is not conserved among the abH03.01 family members and structural conformation of OPE loop α16–α17, in both closed and open states, is also unique (Fig. S3 Supp. Mat.).

Table 2
Percentage of monomer and dimer forms of the esterase, obtained after analytical ultracentrifugation, in protein samples in absence or presence of dodecane sulfonyl chloride, as enzyme inhibitor, and cholesteryl oleate, as enzyme substrate. OPE corresponds to the *O. piceae* esterase expressed in *P. pastoris* after hydrophobic interaction columns. The monomeric fraction was obtained in an additional step by using SEC to separate the different aggregate forms present in the purified protein.

	% monomer	% dimer
OPE	63.1	19.6
OPE + inhibitor	33.4	40.1
OPE + substrate	19.1	71.5
Monomer fraction	69.9	30.1
Monomer fraction + inhibitor	18.6	75.9
Monomer fraction + substrate	16.8	83.2

3.4. The active site cleft and substrate binding

The catalytic machinery of OPE is formed by the triad Ser220, Glu352 and His465. As observed in other members of the fungal family, and unlike other lipases, the acidic residue of the triad is a Glu residue and not an Asp residue. The catalytic region is well conserved between OPE and the other fungal lipases/esterases. The catalytic triad remains unchanged in the open and close conformation of the enzyme. By comparison with homologous enzymes, the backbone NH groups of two Gly residues (Gly134–Gly135) build the oxyanion hole that stabilizes the oxyanion produced in the tetrahedral intermediate generated during the hydrolysis. A water molecule is located close to the oxyanion hole. The oxyanion is the intermediate formed in the transient state of the hydrolysis reaction. Different molecules of PEG from the crystallization condition (see Section 2) were identified occupying the hydrophobic active site cleft, very likely mimicking the position of substrate (Fig. 3a).

The phospholipid molecule attached to the groove leading to the OPE active site was found in both chains of OPE^{o} and presented an excellent electron density (Fig. 2 and Fig. S5 Supp. Mat.) This is the first time in this family of lipases/esterases, that a potential

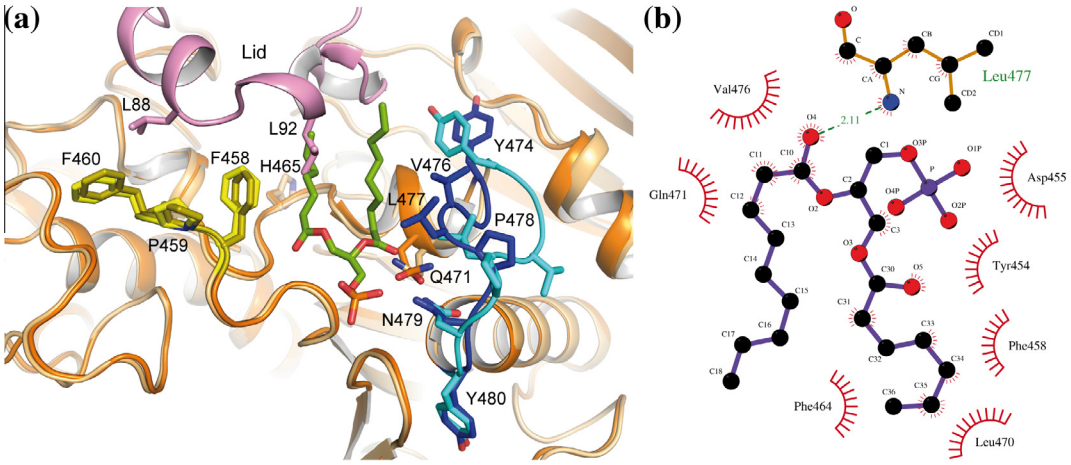

Fig.2. Phospholipid site and recognition in active OPE. (a) The phospholipid (green sticks) is located in a groove formed by the α16–α17 loop (in blue) and the hydrophobic patch (in yellow). Residues involved in substrate stabilization are labeled. Lid from the closed conformation is colored in pink. (b) Schematic representation of the interactions between the phospholipid and the active OPE.

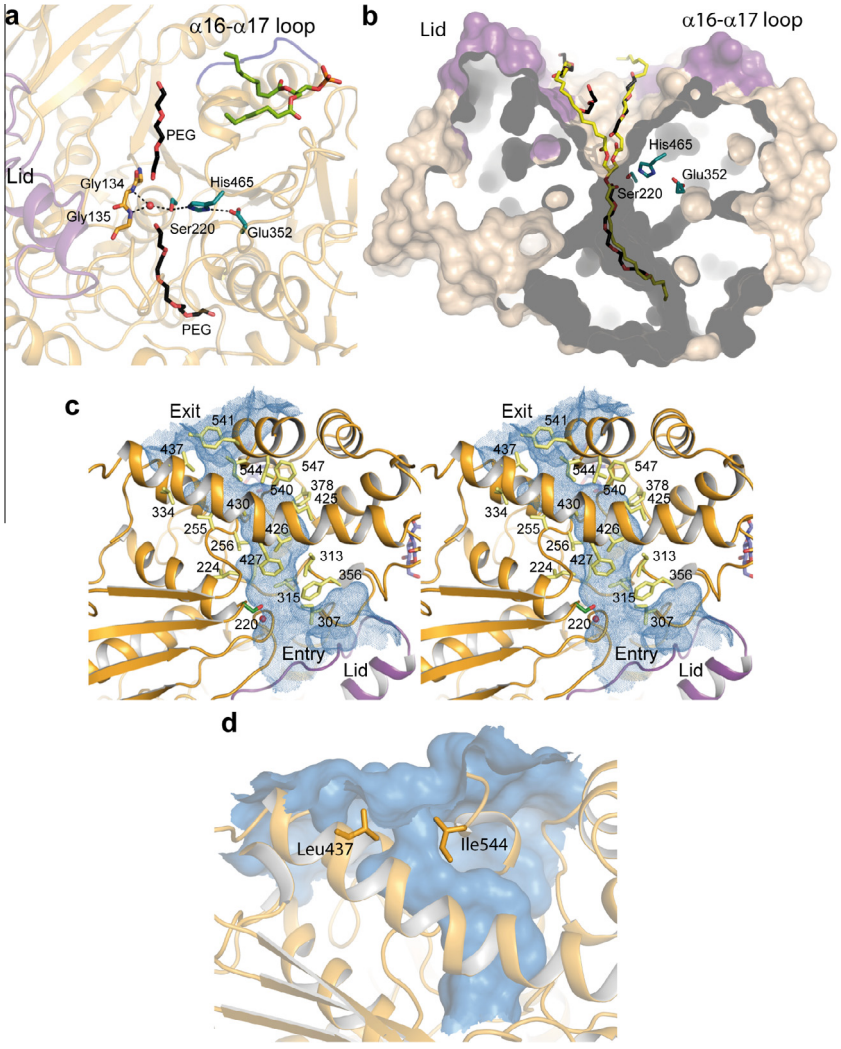

Fig.3. The active site and internal tunnel in OPE. (a) OPE Structural rearrangements upon activation. Molecular surface of OPE (brown) with the catalytic Ser residue highlighted in red. Changes from the closed (inactive state) to open (active state) structures are represented; lid and α16–α17 loop in the closed state are colored in blue; same regions in the open state in purple. Upon activation, structural rearrangements imply a 30 Å displacement of the lid to unmask the catalytic site. The hydrophobic patch is shown in yellow sticks and the phospholipid (green sticks) can be seen in between this region and the α16–α17 loop. Close to the catalytic serine there is an internal tunnel that contains a PEG chain (black sticks). (b) Surface representation of the substrate binding site of OPE. The catalytic triad (Ser220, Glu352, His465) is represented as green sticks. PEG moieties are represented as black sticks. The structure of a triglyceride in a fork conformation (tristearoylglycerol, yellow sticks) is superimposed. (c) Stereo view of the surface of the OPE tunnel (colored in blue) leading from the catalytic site to the exit. Residues lining the tunnel are represented as yellow sticks and labeled. Catalytic serine is shown in green sticks. (d) Narrowing of the OPE internal tunnel is produced by Leu437 and Ile544 (orange sticks).

substrate (phospholipid), is localized in a channel leading to the active site. This groove is built by the α16–α17 loop and the previously described hydrophobic patch. The phospholipid is ensconced by hydrophobic interactions with residues from the α16–α17 loop (Val476 and Leu477) and with Phe458 from the hydrophobic patch. The glycerol moiety of the phospholipid is stabilized by polar interactions with Asp455, Gln471 and Asn479 from the α16–α17 loop (Fig. 2). The observed groove in OPE^o does not exist in the structure of other homologous enzymes for which a Trp or Phe residue fills the cavity in *C. rugosa* and *G. candidum* lipases, respectively (Fig. S3e Supp. Mat.).

3.5. The internal tunnel

OPE^o esterase presents a substrate binding-site formed by an extensive hydrophobic pocket (residues Tyr76, Tyr143, Tyr144, Leu355, Phe458, Leu461, Phe464, Ile469, Leu470 and Tyr474) with a narrow internal tunnel in which aliphatic chains can be stabilized. Different elongated electron densities were observed in both chains (A and B) of the OPE^o active site that were modeled as PEG molecules from the crystallization condition (Fig. 3b). Interestingly some of these chains superimpose with the structure of a triglyceride in a fork conformation with the central aliphatic chain entering into the internal tunnel (Fig. 3b). The PEG molecule stabilized in the tunnel presents a well-defined electron density for a chain of 16 atoms (Fig. S6 Supp. Mat.). Noteworthy, this 30 Å-long internal tunnel connects the active site cleft to the outside at the opposite side (Fig. 3c and Fig. S7 Supp. Mat.). Internal tunnel is formed by aromatic and aliphatic residues that confer a high hydrophobic environment all along it (Fig. 3c). There is a narrowing produced between Leu437 and Ile544 residues (Fig. 3d), the average width in the tunnel being 9 Å and 5.5 Å in the narrowing.

Comparison with the structures of the other abH03.01 members shows that *C. rugosa* lipases Lip1, PDB code 1CRL (Grochulski et al., 1993), Lip2, PDB code 1GZ7 (Mancheño et al., 2003) and Lip3, PDB code 1CLE (Ghosh et al., 1995), present a similar tunnel but oriented towards a different region of the protein surface (Fig. S7b Supp. Mat.). Lipase from *G. candidum* displays also a tunnel, similarly oriented than *C. rugosa* lipases, but with different narrowing along the tunnel (Fig. S7c Supp. Mat.). The esterase from *A. niger*

completely lacks the tunnel (Fig. S7d Supp. Mat.). In this sense, it is worth to note how proteins sharing a similar overall structure (Fig. S3 Supp. Mat.) can display strong differences concerning its internal tunnel. As revealed by structural analysis, small changes in amino acid composition and/or rotamers can result in a completely different structural arrangement of the tunnel, e.g., while the first half of the tunnel follows the same path in *O. piceae*, in *C. rugosa* and *G. candidum* lipases, a substitution of a serine by Tyr377 in OPE blocks the path redirecting it about 150° apart (Fig. S7 Supp. Mat.).

In an attempt to ascertain the potential role of the tunnel in the product release of the reaction, we constructed a site-directed mutant, replacing Ile544 by a Trp residue (OPE-I544W). The goal with this mutant was to block the substrate exit by inserting a bulky hydrophobic residue. The OPE-I544W mutant was purified and its structure solved at 2.4 Å resolution (Table 1). Both native and mutated proteins showed no differences in their secondary structure (rmsd of 0.147 Å for 518 Cα atoms). As expected, substitution of Ile544 residue by bulky Trp residue completely blocks the potential exit of the internal tunnel (Fig. 4).

Different activity studies were carried out comparing wild type *versus* mutated enzyme (Fig. 4b). Our results (Table 3) show that while enzyme activity against *p*NPB and *p*NPL was similar in the mutated and wild type enzymes, the activity was completely lost with *p*NPP (~0.2% of the wt enzyme). These results suggest that the length of the substrate affects the activity of the mutated protein at the end of the tunnel; while short-medium substrates (4 and 12 C atoms) remain mostly unaffected, hydrolytic activity with substrates having more than 16 C atoms is severely reduced *versus* that of wt.

On the other hand, amino acid composition in the internal tunnel of *C. rugosa* lipases has been associated to differences in substrate specificity between Lip1 and Lip3 (Ghosh et al., 1995). Structural comparison among the three *C. rugosa* isoenzymes (Lip1, Lip2 and Lip3) has been reported to show two distinctive regions according to their amino acid composition: an aromatic-rich region at the beginning of the tunnel and an aliphatic-rich region at the bottom (Mancheño et al., 2003). Whereas this second region remained essentially identical in the three isoenzymes and thus the interactions with the alkyl chains of the substrates would be very similar, the phenylalanine content of the first region differs in the three proteins (Mancheño et al., 2003), a fact that was associated with the substrate recognition properties of the isoenzymes, namely, to their lipase/esterase character. The differences of *C. rugosa* lipases activity on cholesterol esters (Lip2 > Lip3 > Lip1) have been related to the higher Phe content in the hydrophobic region of the tunnel (Lip1 > Lip3 > Lip2) (Mancheño et al., 2003). In the case of OPE, the Phe content in this region is similar to

Table 3
Specific activity of the recombinant protein expressed in *P. pastoris*, as well as on the mutant I544W constructed by site-directed mutagenesis, on 2 mM *p*NPB, *p*NPL and *p*NPP, in presence of 1% genapol.

Substrate	Fatty acids	Specific activity (U mg^{-1})	
		OPE native	I544W
*p*NPB	C4:0	103.17 ± 2.54	113.44 ± 3.52
*p*NPL	C12:0	162.72 ± 6.82	203.65 ± 12.93
*p*NPP	C16:0	65.78 ± 5.30	0.13 ± 0.013

Lip2. It could explain its ability to hydrolyze sterol esters. However, its high efficiency, when compared to the commercial *C. rugosa* cholesterol esterase to hydrolyze triglycerides with long chain fatty acids or different cholesterol esters (Calero-Rueda et al., 2009), could be related to its specific internal tunnel and its unique dimeric structure. The presence of large opening in the active dimer could allow the entrance of different substrates that can be stabilized in the 30 Å-long internal tunnel.

3.6. Proposed model of substrate entry and product release in OPE

Crystal structures of OPE provide clues about the fate of the substrate to be hydrolyzed by the enzyme. The closed conformation of OPE is a monomer with the large lid masking the active site. Activation involves both, opening of the lid and the rearrangement of α16–α17 loop and the formation of a dimeric structure. As proven by our experiments, isolation of the monomeric form results in an increase of the dimer upon activation of the enzyme. Once the lid is open, the hydrophobic surface behind it is exposed, allowing the substrate to move to the catalytic cleft where the catalytic Ser220 residue is located. The hydrocarbon chain of the substrate is inserted into the tunnel up to the point at which the ester bond reaches the Ser220. After reaction, the acidic moiety of the ester (a fatty acid) could remain in the tunnel, while the sterol moiety is released. The fatty acid inside the tunnel has to be released in order to recover the active state of the enzyme.

Our mutagenesis experiments indicate that a single modification blocking the exit of the tunnel 30 Å far from active site (by replacing Ile544 by bulky Trp residue) did not affect significantly the OPE activity on substrates with short-medium chain fatty acids. While an appealing hypothesis is that substrates could be released by the exit of the tunnel, our crystallographic and biochemical experiments indicate that the exit of the tunnel is not required for efficient hydrolysis in OPE against these substrates. The observed lost of activity of the OPE I544W mutant with *p*NPP could be explained by the presence of bulky Trp residue at the end of the tunnel that decreases its effective length avoiding the right

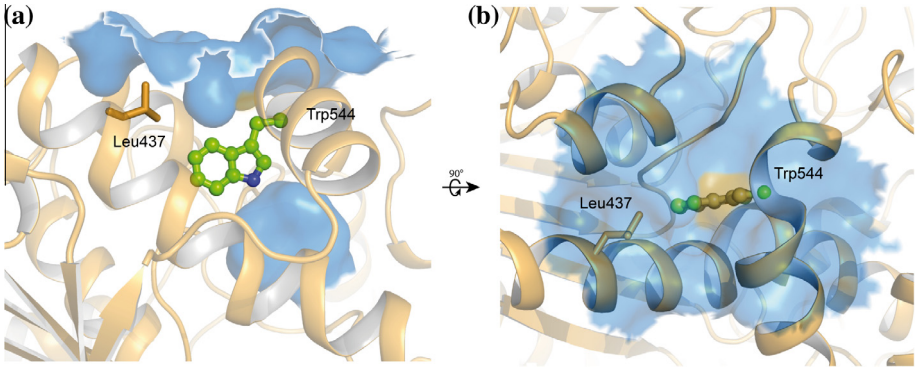

Fig.4. Blocking tunnel exit by site directed mutagenesis. (a) View of the molecular surface in the OPE I544W mutant (b) the molecular surface of the OPE mutant rotated 90°. The mutation blocks the potential exit of the tunnel (surface for the mutated position is colored in orange on the right panel).

positioning of long substrates to be cleaved at catalytic site. This has been observed in the cholesterol esterase Lip3 from *C. rugosa* where the cholesteryl linoleate ligand was found with the aliphatic chain entering into the internal tunnel orienting the cholesteryl moiety to be cleaved by catalytic Ser residue (Fig. S7 Supp. Mat.). Therefore the length and amino acid composition of the internal tunnel seems to be crucial to understand the catalytic versatility of OPE. The other essential parameter is the dimeric nature of the active form. Contrary to the previously observed dimer in the cholesterol esterase Lip3 from *C. rugosa*, that presented a tight homodimer with small cavities entering into the active sites (Fig. S9 Supp. Mat.), the dimer in the OPE^{o} shows a pacman-like structure with a very large opening (23 Å × 38 Å) (Fig. S9 Supp. Mat.) that could allow both the entrance of large substrates and also quick release of the reaction products. Further experiments will be needed to corroborate this hypothesis and study the role of the internal tunnel in this protein for its action on long-chain fatty acids substrates.

4. Conclusion

Here we describe, for the first time, the structural rearrangements required for the activation and degradation mechanism of the OPE cholesterol esterase from abH03.01 family of fungal lipases/esterases. Structural analysis revealed different pockets that, upon activation, are responsible of dimerization and stabilization of the acyl chains of the substrate. Based on our structural and biochemical results, we propose a mechanism by which a great variety of different substrates can be hydrolyzed and released in OPE. These results reveal a new scenario in which not only the activation of the enzyme but also the release of its hydrolysis products could be handled paving the way for the construction of new variants to improve the catalytic properties of these enzymes and their biotechnological applications.

Acknowledgments

This work was supported by Grants BFU2011-25326 and BIO2012-3637 from Spanish Ministry of Economy and Competitiveness and by S2010/BMD-2457 and S-2009AMB-1480 Grants from Autonomous Community of Madrid. M.E. Vaquero thanks the Spanish Ministry of Economy for a FPU fellowship. Authors thank the help of the Analytical Ultracentrifugation CIB facility for ultracentrifugation experiments.

Appendix A. Supplementary data

Supplementary data associated with this article can be found, in the online version, at http://dx.doi.org/10.1016/j.jsb.2014.07.007.

References

Adams, P.D., Afonine, P.V., Bunkoczi, G., Chen, V.B., Davis, I.W., Echols, N., Headd, J.J., Hung, L.W., Kapral, G.J., Grosse-Kunstleve, R.W., McCoy, A.J., Moriarty, N.W., Oeffner, R., Read, R.J., Richardson, D.C., Richardson, J.S., Terwilliger, T.C., Zwart, P.H., 2010. PHENIX: a comprehensive Python-based system for macromolecular structure solution. Acta Crystallogr. D Biol. Crystallogr. 66, 213–221.

Allain, C.C., Poon, L.S., Chan, C.S.G., Richmond, W., Fu, P.C., 1974. Enzymatic determination of total serum-cholesterol. Clin. Chem. 20, 470–475.

Barba Cedillo, V., Plou, F.J., Martinez, M.J., 2012. Recombinant sterol esterase from *Ophiostoma piceae*: an improved biocatalyst expressed in *Pichia pastoris*. Microb. Cell Fact. 11, 1–14.

Barba, V., Prieto, A., Martínez, A.T., Martínez, M.J., 2011. Procedimiento para la obtención de compuestos de interés alimenticio y/o farmacéutico mediante reacciones de acilación de fitoesteroles libres con ácidos grasos catalizadas por una esterol esterasa procedente de hongos del género Ophiostoma. Patent (Spain), P201131098 20, June 2008.

Barriuso, J., Prieto, A., Martínez, M.J., 2013. Fungal genomes mining to discover novel sterol esterases and lipases as catalysts. BMC Genomics 14, 712–719.

Bourne, Y., Hasper, A.A., Chahinian, H., Juin, M., de Graaff, L.H., Marchot, P., 2004. Aspergillus niger protein EstA defines a new class of fungal esterases within the alpha/beta hydrolase fold superfamily of proteins. Structure 12, 677–687.

Calero-Rueda, O., Barba, V., Rodriguez, E., Plou, F., Martínez, A.T., Martínez, M.J., 2009. Study of a sterol esterase secreted by *Ophiostoma piceae*: sequence, model and biochemical properties. Biochim. Biophys. Acta 1794, 1099–1106.

Calero-Rueda, O., Gutiérrez, A., del Río, J.C., Muñoz, C., Plou, F.J., Martínez, A.T., Martínez, M.J., 2002a. Method for the enzymatic control of pitch deposits formed during paper pulp production using an esterase that hydrolyses triglycerides and sterol esters. Patent (International) WO 02/075045 A1.

Calero-Rueda, O., Plou, F.J., Ballesteros, A., Martínez, A.T., Martínez, M.J., 2002b. Production, isolation and characterization of a sterol esterase from *Ophiostoma piceae*. BBA Proteins Proteomics 1599, 28–35.

Emsley, P., Lohkamp, B., Scott, W., Cowtan, K., 2010. Features and development of Coot. Acta Crystallogr. D Biol. Crystallogr. 66, 486–501.

Evans, P., 2006. Scaling and assessment of data quality. Acta Crystallogr. D Biol. Crystallogr. 62, 72–82.

Ghosh, D., Wawrzak, Z., Pletnev, V.Z., Li, N., Kaiser, R., Pangborn, W., Jörnvall, H., Erman, M., Duax, W.L., 1995. Structure of uncomplexed and linoleate-bound *Candida cylindracea* cholesterol esterase. Structure 3, 279–288.

Grochulski, P., Li, Y.G., Schrag, J.D., Bouthillier, F., Smith, P., Harrison, D., Rubin, B., Cygler, M., 1993. Insights into interfacial activation from an open structure of *Candida rugosa* lipase. J. Biol. Chem. 268, 12843–12847.

Grochulski, P., Li, Y., Schrag, J.D., Cygler, M., 1994. 2 conformational states of *Candida-rugosa* lipase. Protein Sci. 3, 82–91.

Hermoso, J., Pignol, D., Kerfelec, B., Crenon, I., Chapus, C., FontecillaCamps, J.C., 1996. Lipase activation by nonionic detergents – the crystal structure of the porcine lipase–colipase–tetraethylene glycol monooctyl ether complex. J. Biol. Chem. 271, 18007–18016.

Hermoso, J., Pignol, D., Penel, S., Roth, M., Chapus, C., FontecillaCamps, J.C., 1997. Neutron crystallographic evidence of lipase–colipase complex activation by a micelle. EMBO J. 16, 5531–5536.

Ho, B.K., Gruswitz, F., 2008. HOLLOW: generating accurate representations of channel and interior surfaces in molecular structures. BMC Struct. Biol., 8.

Holmquist, M., 2000. Alpha/beta-hydrolase fold enzymes: structures, functions and mechanisms. Curr. Protein Pept. Sci. 1, 209–235.

Houde, A., Kademi, A., Leblanc, D., 2004. Lipases and their industrial applications – an overview. Appl. Biochem. Biotechnol. 118, 155–170.

Kabsch, W., 2010. Xds. Acta Crystallogr. D Biol. Crystallogr. 66, 125–132.

Kontkanen, H., Tenkanen, M., Reinikainen, T., 2006. Purification and characterisation of a novel steryl esterase from *Melanocarpus albomyces*. Enzyme Microb. Technol. 39, 265–273.

Maeda, A., Mizuno, T., Bunya, M., Sugihara, S., Nakayama, D., Tsunasawa, S., Hirota, Y., Sugihara, A., 2008. Characterization of novel cholesterol esterase from *Trichoderma* sp. AS59 with high ability to synthesize steryl esters. J. Biosci. Bioeng. 105, 341–349.

Mancheño, J.M., Pernas, M.A., Martínez, M.J., Ochoa, B., Rua, M.L., Hermoso, J.A., 2003. Structural insights into the lipase/esterase behavior in the *Candida rugosa* lipases family: crystal structure of the lipase 2 isoenzyme at 1.97 A resolution. J. Mol. Biol. 332, 1059–1069.

McCoy, A.J., Grosse-Kunstleve, R.W., Adams, P.D., Winn, M.D., Storoni, L.C., Read, R.J., 2007. Phaser crystallographic software. J. Appl. Crystallogr. 40, 658–674.

Morinaga, N., Maeda, A., Mizuno, T., Bunya, M., Sugihara, S., Sugihara, A., 2011. Synthesis of fatty acid sterol esters using cholesterol esterase from *Trichoderma* sp. AS59. Enzyme Microb. Technol. 48, 498–504.

Ollis, D.L., Cheah, E., Cygler, M., Dijkstra, B., Frolow, F., Franken, S.M., Harel, M., Remington, S.J., Silman, I., Schrag, J., Sussman, J.L., Verschueren, K.H.G., Goldman, A., 1992. The alpha/beta-hydrolase fold. Protein Eng. 5, 197–211.

Rahim, M.A., Sih, C.J., 1969. Microbial steroid esterases. Methods Enzymol. 15, 675–684.

Reetz, M.T., 2002. Lipases as practical biocatalysts. Curr. Opin. Chem. Biol. 6, 145–150.

Schrag, J.D., Cygler, M., 1993. 1.8-Angstrom refined structure of the lipase from *Geotrichum-candidum*. J. Mol. Biol. 230, 575–591.

Schrödinger, L., 2010. The PyMOL Molecular Graphics System, Version 1.2r2′.

Schuck, P., 2000. Size-distribution analysis of macromolecules by sedimentation velocity ultracentrifugation and Lamm equation modeling. Biophys. J. 78, 1606–1619.

Singh, A.K., Mukhopadhyay, M., 2012. Overview of fungal lipase: a review. Appl. Biochem. Biotechnol. 166, 486–520.

Turner, N.A., Needs, E.C., Khan, J.A., Vulfson, E.N., 2001. Analysis of conformational states of *Candida rugosa* lipase in solution: Implications for mechanism of interfacial activation and separation of open and closed forms. Biotechnol. Bioeng. 72, 108–118.

Verger, R., 1997. Interfacial activation of lipases: fact and artifacts. Trends Biotechnol. 15, 32–38.

Winn, M.D., Ballard, C.C., Cowtan, K.D., Dodson, E.J., Emsley, P., Evans, P.R., Keegan, R.M., Krissinel, E.B., Leslie, A.G., McCoy, A., McNicholas, S.J., Murshudov, G.N., Pannu, N.S., Potterton, E.A., Powell, H.R., Read, R.J., Vagin, A., Wilson, K.S., 2011. Overview of the CCP4 suite and current developments. Acta Crystallogr. D Biol. Crystallogr. 67, 235–242.